VIP Magnetic Materials Very Important Paper

International Edition: DOI: 10.1002/anie.201511436
German Edition: DOI: 10.1002/ange.201511436

Superparamagnetic Reduced Graphene Oxide with Large Magnetoresistance: A Surface Modulation Strategy

Jing Peng[+], Yuqiao Guo[+], Haifeng Lv, Xinyu Dou, Qi Chen, Jiyin Zhao, Changzheng Wu, Xiaojiao Zhu, Yue Lin, Wei Lu, Xiaojun Wu, and Yi Xie*

Abstract: *The graphene system is actively pursued in spintronics for its nontrivial sp electron magnetism and its potential for the flexible surface chemical tuning of magnetoelectronic functionality. The magnetoresistance (MR) of graphene can be effectively tuned under high magnetic fields at cryogenic temperatures, but it remains a challenge to achieve sensitive magnetoelectric response under ambient conditions. We report the use of surface modulation to realize superparamagnetism in reduced graphene oxide (rGO) with sensitive magnetic field response. The superparamagnetic rGO was obtained by a mild oxidation process to partially remove the thiol groups covalently bound to the carbon framework, which brings about large low-field negative MR at room temperature (−8.6 %, 500 Oe, 300 K). This strategy provides a new approach for optimizing the intrinsic magnetoelectric properties of two-dimensional materials.*

Two-dimensional (2D) nanomaterials that display spin-polarized effects are promising for the reduction in size of electronic components and flexible surface chemical tuning of magnetoelectronic functionality.[1] Spin polarization in 2D nanomaterials has been realized by surface chemical modification, anionic substitution, and defect engineering,[2] which result in remarkable changes to electronic transport properties under external magnetic fields. However, achieving large magnetoresistance (MR) under low magnetic fields at ambient conditions in 2D nanomaterials still remains a challenge that is critical for practical applications. Superparamagnetic (SPM) structures, in which the magnetic domains of ferromagnetic (FM) materials are reduced to a critical size so that they can flip independently, could be an effective way to achieve large MR under low external magnetic fields.[3] Although this type of SPM structure has been realized for zero-dimensional nanoparticles, it has not been reported to date for 2D nanomaterials.

Reduced graphene oxide (rGO), which is a 2D material with nontrivial sp electron magnetism,[4] is a chemically tunable platform for realizing SPM structure. Many functional groups can be covalently bound both on the basal plane and at the edges of rGO,[5] and room-temperature ferromagnetism arising from these functional groups has been confirmed.[6] Since the magnetic properties are sensitive to the alteration of these groups, SPM structure can be expected if the magnetic domain of ferromagnetic rGO is reduced to a critical size by modulating the topological distribution of the functional groups. Theoretical calculations have showed that thiol groups in rGO can induce localized magnetic moments,[7] and room-temperature ferromagnetism was experimentally observed in thiol-containing rGO.[8] Considering that thiol groups on rGO are highly active under ambient conditions because of their reductivity, the surface density of thiol groups can be easily modulated by external stimuli such as oxygen, and as a result the magnetic domain size of thiol-containing rGO can be tuned by changing the topological distribution of thiol groups. Therefore, the superparamagnetic rGO may show large MR effects under low magnetic fields at room temperature.

Herein, we report a reduced graphene oxide with an SPM structure, as a new graphene-based magnetoelectric system that shows a large low-field negative MR effect at room temperature. The superparamagnetic rGO, with noninteracting magnetic domains induced by thiol groups that are covalently bound to the carbon framework, triggers a highly sensitive response to magnetic fields at room temperature (MR value: −8.6 %, 500 Oe, 300 K). The large MR effect is ascribed to the increased electron transport probability accompanied by the alignment of independent magnetic domains under external magnetic fields. In this case, the MR effect in superparamagnetic rGO behaves as a novel magneto-transport model with a strong coupling of structure, spin, and charge in a 2D electron transport system. The transformation from ferromagnetism to superparamagnetism depends on the structural evolution by the gradual removal

[*] J. Peng,[+] Y. Q. Guo,[+] H. F. Lv, X. Y. Dou, J. Y. Zhao, Prof. C. Z. Wu, X. J. Zhu, Y. Lin, Prof. X. J. Wu, Prof. Y. Xie
Hefei National Laboratory for Physical Sciences at the Microscale
iChEM (Collaborative Innovation Center of Chemistry for Energy Materials), Hefei Science Center (CAS) and CAS Key Laboratory of Mechanical Behavior and Design of Materials
University of Science & Technology of China
Hefei 230026 (PR China)
E-mail: czwu@ustc.edu.cn

H. F. Lv, Prof. X. J. Wu
CAS Key Lab of Materials for Energy Conversion
Department of Materials Science and Engineering
University of Science & Technology of China
Hefei 230026 (PR China)

Q. Chen, Prof. W. Lu
i-Lab, Suzhou Institute of Nano-Tech and Nano-Bionics
Chinese Academy of Sciences
Suzhou 215123 (PR China)

[+] These authors contributed equally to this work.

Supporting information for this article is available on the WWW under http://dx.doi.org/10.1002/anie.201511436.

of thiol groups in reduced graphene oxide. In our case, high-sulfur-concentration rGO (HS-rGO) was obtained by direct reaction of graphene oxide (GO) with hydrogen sulfide gas in the reaction $GO + H_2S \rightarrow HS\text{-}rGO + H_2O$. Low-sulfur-concentration rGO (LS-rGO) was produced by very mild oxidation with oxygen gas, partly removing the thiol groups from HS-rGO and form LS-rGO. Despite the similar graphene framework for both HS-rGO and LS-rGO, changing the number of thiol groups bonded to rGO triggers the change of magnetic structure (Figure 1 a).

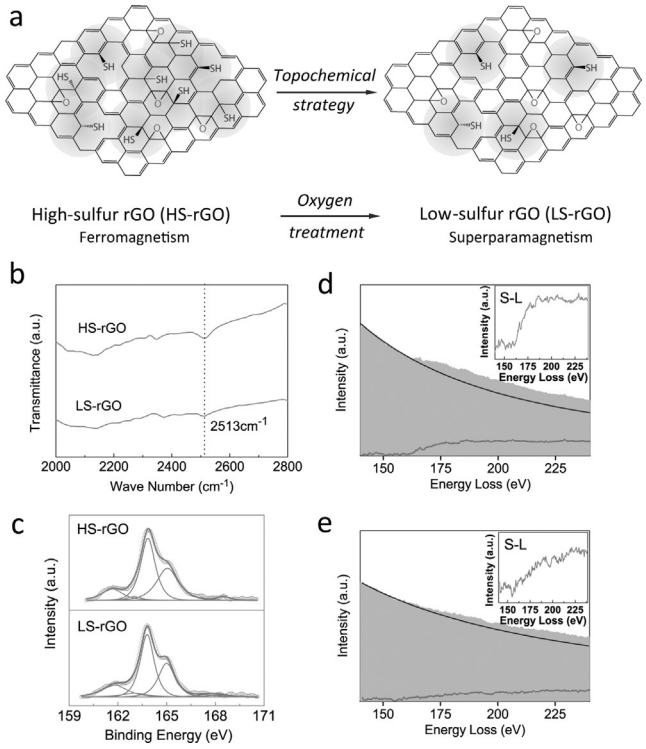

Figure 1. Chemical composition and structural characterization of HS-rGO and LS-rGO nanosheets. a) Chemical and magnetic structures in high-sulfur-concentration rGO (HS-rGO) and low-sulfur-concentration rGO (LS-rGO). b) FTIR spectra. c) XPS S 2p spectra. d, e) EELS spectra of the sulfur L-edge. The respective expansions are shown as insets.

Raman spectra were recorded to probe the fine structural changes during the reaction. As shown in Figure S1 a in the Supporting Information, Raman spectra showed that both HS-rGO and LS-rGO have a similar rGO framework, with the D-band and G-band at similar wavelengths and similar full width at half maximum values (FWHM; see Supplementary Table S1), revealing no obvious structural change to the graphene framework.[9] However, further characterization, including Fourier transform infrared spectroscopy (FTIR) spectra, X-ray photoemission spectroscopy (XPS), and electron energy loss spectra (EELS), clearly verified the reduction in the number of thiol groups from HS-rGO to LS-rGO. As seen in the FTIR spectra (Figure 1 b), an apparent characteristic absorption peak of the S–H groups ($2513\ cm^{-1}$) can be seen in HS-rGO. By comparison, only a weak S–H signal can be observed in the spectrum of LS-rGO, thus indicating the content of thiol groups in HS-rGO is probably higher than that of LS-rGO. XPS was also utilized to investigate the change of chemical components before and after oxidation of HS-rGO (Figure 1 c and Figure S1). The main peaks at 164.0 eV and 165.2 eV can be attributed to the doublet peaks of the S 2p spectrum in the S–H bond.[10] In our case, the different C/S–H (i.e., carbon/thiol) ratio can be observed after subtracting the Shirley background. As seen in Table S1, the C/S–H ratio increases from 32.6 in HS-rGO to 64.0 in LS-rGO with an enhanced proportion of epoxy groups, thus indicating that some of the thiol groups in HS-rGO transformed into epoxy groups when exposed to oxygen gas, and that LS-rGO nanosheets have fewer thiol groups than HS-rGO. EELS was used to give further evidence for the decrease in the amount of thiol groups, and was performed to study the microscopic phase variation of individual nanosheet. Figure 1 d and 1 e show the sulfur L-edge from HS-rGO and LS-rGO, respectively. The signal intensity for HS-rGO is higher than that of the LS-rGO, which further demonstrates that the sulfur content is lower in LS-rGO. These evidences confirm that HS-rGO and LS-rGO are both based on rGO structures with thiol groups covalently incorporated in the carbon framework, but HS-rGO has a higher thiol density than LS-rGO.

Spin configurations of the samples were detected by using magnetometry on a superconducting quantum interference device magnetometer (SQUID). The field-dependent hysteresis loop (M–H) curves of the HS-rGO and LS-rGO at 300 K are shown in Figure 2 a and 2 b, respectively. The S-shaped M–H curves with obvious hysteresis behavior for the HS-rGO sample clearly demonstrate its room-temperature ferromagnetism and the saturation magnetization and coercivity field extracted from the M–H curve were $0.065\ emu\ g^{-1}$ and 120 Oe, respectively (inset in Figure 2 a). However, for the LS-rGO samples as shown in Figure 2 b, although a similar S-shaped curve was also observed, the negligible remanent magnetization and coercivity in hysteresis loops (inset in Figure 2 b) indicate SPM behavior. Similar behavior is usually observed in some FM nanoparticles, where the magnetization of a single nanoparticle can be regarded as an independent magnetic domain. Although both FM and SPM states consist of magnetic domains, unlike the strong magnetic interaction between the neighboring magnetic domains in FM solids, there is negligible magnetic interaction between the neighboring magnetic domains in those SPM systems. The above results demonstrate that the SPM state was successfully obtained in LS-rGO. Magnetic force microscopy (MFM) provides a powerful tool for directly obtaining magnetic signals in local microstructures,[11] and in our case MFM was used to directly measure the corresponding magnetic response of HS-rGO and LS-rGO nanosheets. As shown in Figure 2 c–f and Figure S2, MFM measurements for the HS-rGO nanosheets showed a simultaneous increase in phase and amplitude, thus demonstrating a repulsive force between the HS-rGO and the MFM tip and hence confirming that the HS-rGO nanosheets are microscopically magnetic.[12] The magnetic response obtained for the LS-rGO nanosheet was rather weaker than that of HS-rGO (Figure 2 g–j), which is in good agreement with the SQUID results.

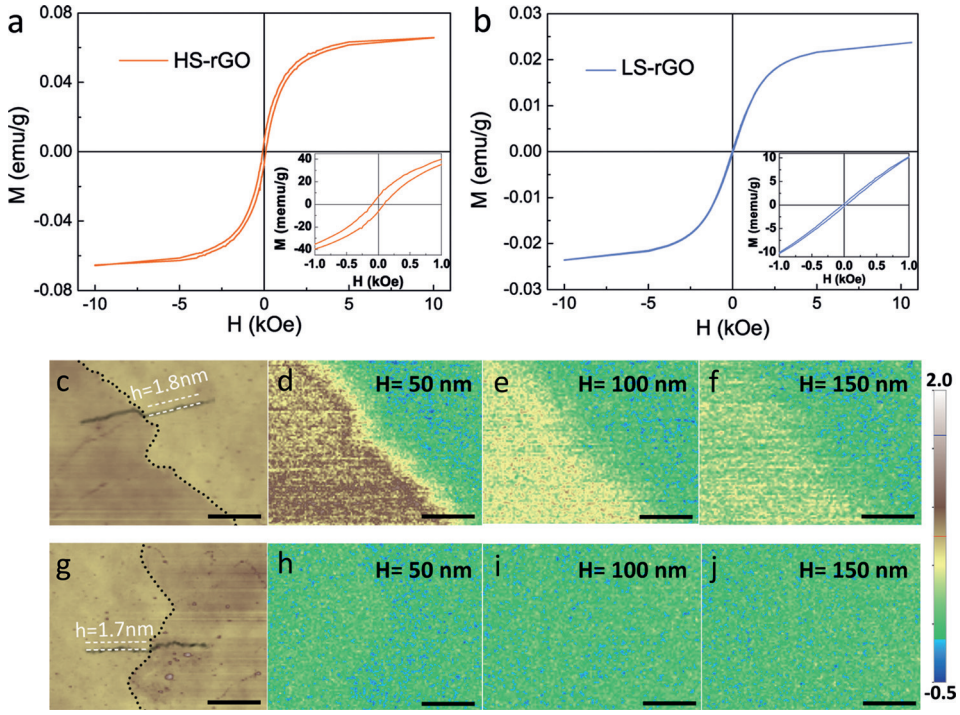

Figure 2. Magnetic properties of HS-rGO and LS-rGO. Field-dependent magnetization (M–H curve) at 300 K for a) HS-rGO and b) LS-rGO nanosheets, respectively, the insets shows the magnified views of the low-field region. c–j) MFM images of HS-rGO and LS-rGO nanosheets. (c, g) show AFM topography. Dashed black lines show the edge of nanosheets. (d, e, f) and (h, i, j) show MFM phase images of HS-rGO (upper) and LS-rGO (lower) with lift heights of 50, 100, 150 nm, respectively. Scale bar = 1 μm.

In order to investigate the magnetotransport behavior of HS-rGO and LS-rGO nanosheets, standard four-terminal nanosheet devices (Figure S3a) in a commercial physical property measurement system (PPMS; see the Supporting Information for details) were used. Figure 3a and 3b show the typical temperature-dependent resistivity of the HS-rGO and LS-rGO nanosheets with three atomic layers under a series of external perpendicular magnetic fields ranging from 0 to 1 Tesla, respectively (for broader temperature-dependent resistivity see Figures S3b and S3c). Different magnetotransport behaviors are observed: LS-rGO has a large negative magnetic field coefficient of resistivity, while HS-rGO has a negligible value. The field-dependent MR for HS-rGO and LS-rGO are plotted in Figure 3c and 3d, respectively. Here, the field-dependent MR is defined as MR(H) % = $[\rho(H)-\rho(0)]/\rho(0)$, where $\rho(H)$ and $\rho(0)$ are the resistivity under the magnetic field H and zero field, respectively. The MR value of HS-rGO was rather small at room temperature; however, LS-rGO exhibited large negative MR at the same temperature. For LS-rGO, the external magnetic field greatly suppressed electrical resistivity under a very low magnetic field: For instance, the negative MR values were as large as −8.6% under 500 Oe and −14.9% under 1 T at 300 K, as depicted in Figure 3d. Moreover, the MR curve of LS-rGO exhibits two distinct regions: the low-field region (within 2000 Oe) where the MR shows a rapid increase with the magnetic field, and the high-field region (above 2000 Oe), where the MR displays a much slower increase with the field. Furthermore, the coercivity field and MR value can be modulated by the oxygen-treatment time as shown in Figure S4, and finally both of them reached a saturated value. The reduced graphene oxide (rGO) nanosheets with superparamagnetic properties (LS-rGO) show a large low-field negative MR effect at room temperature (−8.6%, 500 Oe, 300 K), representing a new graphene-based magnetoelectric system.

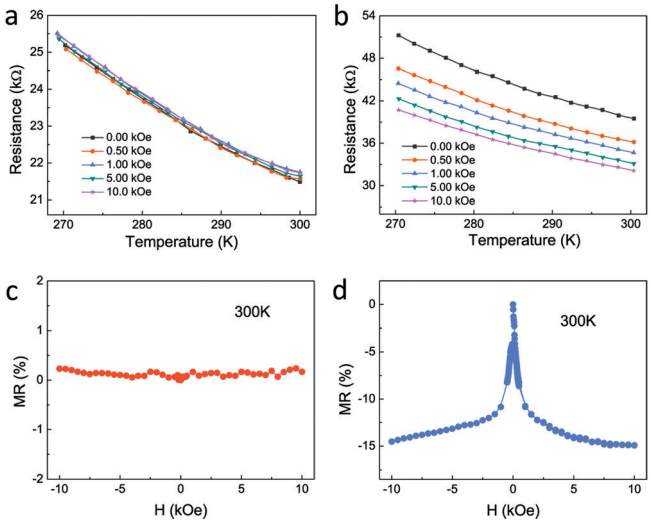

Figure 3. Magnetotransport properties of HS-rGO and LS-rGO. Temperature-dependent resistance under various magnetic fields at the temperature range from 270 K to 300 K for a) HS-rGO and b) LS-rGO, respectively. Magnetic-field dependence of the MR for c) HS-rGO and d) LS-rGO at 300 K.

First-principles spin-restricted calculations using the Vienna Ab Initio Simulation Package[13] (VASP) provided further help to understand the magnetic structure derivation and evolution of the rGO samples. Thiol groups cannot be directly chemisorbed on perfect graphene unless surface defects are present, such as vacancies, Stones–Wales defects, and adatoms.[7] We simulated two possible models: thiol chemisorbed on graphene with the assistance of 1) carbon vacancies, and 2) oxygen adatoms. The theoretical calculations showed that both structures can be thermodynamically stable at room temperature. Further calculations indicated that these two structures can introduce permanent magnetic moments, which originate from the thiol groups, as can be

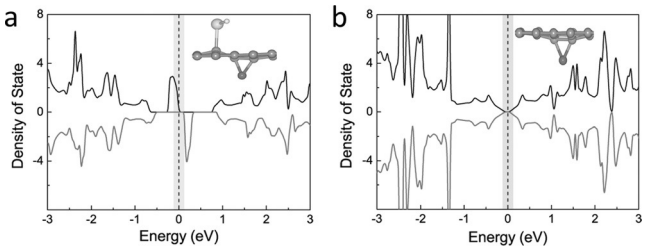

Figure 4. Origin of the magnetic properties and magnetotransport in HS-rGO and LS-rGO. (a) DOS of the structure with a thiol group chemisorbed on graphene and the assistance of an epoxy group; (b) DOS of the structure with only an epoxy group (and no thiol group) on the graphene sheet.

seen from the total density of states (DOS) shown in Figure 4a and Figure S5a. However, for structure (2), the thiol radical is desorbed when the oxygen molecule reacts with the thiol group and the reaction process is theoretically spontaneous at 300 K with a small energy barrier of only 0.1 eV (Figure S5b). As a consequence, the structure becomes nonmagnetic with desorption of the thiol groups (Figure 4b). In contrast, the reaction of structure (1) is limited by an activation barrier of 0.88 eV, which is much higher than that for the reaction of thiols with oxygen atoms, and the barrier is high enough as to impede desorption of thiol groups at ambient condition (see Supplementary Figure S5c). Therefore, the combined experimental and theoretical results show that the resulting concentrations of magnetic centers determine the magnetic ordering: when they are in high concentrations and close to each other, they undergo room-temperature magnetic ordering to form ferromagnetic HS-rGO. In contrast, after treatment with oxygen, the concentration of thiol radicals is gradually reduced to a low level, and only those thiol groups attached to vacancies survive and contribute to the separated magnetic moments in LS-rGO. In our case, the declining concentration of unpaired spins means that the magnetic coupling between magnetic moments decays and the magnetic domains reach a critical size to result in superparamagnetism.

The SPM structure is essential for a high magnetoresponse as the magnetic domains can switch their field direction at low fields as shown by the rapid increase in the magnetization. The electron transport in the sample is affected by the relative angle of the neighboring magnetization directions and the transport capacity reaches a maximum when the spins of the neighboring domains are parallel.[14] As a result, when the external magnetic field is applied, the neighboring independent magnetic domains become aligned in a parallel arrangement along the field direction, which increases the electron tunneling probability. When the applied field reaches the saturation field (2000 Oe), all the small magnetic domains are almost fully aligned with the field direction and the rapid MR increase reaches saturation simultaneously (Figure 3d). We suggest that the low-field MR (less than 2000 Oe) in the LS-rGO comes from the increased electron-transport probability accompanied by the alignment of independent ferromagnetic domains under the external magnetic field. Above the saturation field (2000 Oe), the magnetization increases slowly with field because of the suppression of magnetic-moment fluctuation under high magnetic field. A pronounced MR effect was not observed for HS-rGO, in that the domain size in HS-rGO is much larger than that of the SPM counterpart and even larger than the mean free path of electrons and hence the arrangement of FM domains has a negligible impact on the electron-transport properties of the sample. Therefore, HS-rGO with an FM structure shows negligible MR effect while LS-rGO with an SPM structure shows large low-field negative MR at room temperature.

In conclusion, we have reported a graphene magnetoelectric system, namely reduced graphene oxide (rGO) with an SPM structure, which shows a large low-field negative MR effect at room temperature. The LS-rGO with independent magnetic domains was realized by modulating the topological domain distribution induced by the thiol groups covalently bound to the carbon framework. When the proportion of thiol radicals is reduced, the number of unpaired spins decreased and the magnetic domains were reduced to a critical size so as to obtain an SPM structure with sensitive magnetoelectric response under ambient conditions. We anticipate that this two-dimensional superparamagnetic structure provides a new paradigm for the construction of magnetoelectric materials for two-dimensional systems.

Acknowledgements

We would like to thank Dr. Lin-Jun Wang (USTC Center for Micro- and Nanoscale Research and Fabrication) for valuable discussions about the focused ion beam (FIB) fabrication. This work was financially supported by the National Basic Research Program of China (2015CB932302), the National Natural Science Foundation of China (21222101, 21501164, U1432133, 11132009, 21331005, 11321503, J1030412), National Young Top-Notch Talent Support Program, the Chinese Academy of Sciences (XDB01020300), the Fok Ying-Tong Education Foundation, China (Grant No.141042), and the Fundamental Research Funds for the Central Universities (WK2060190027, WK2340000065).

Keywords: magnetic properties · magnetoresistance · reduced graphene oxide · superparamagnetism · surface modulation

How to cite: *Angew. Chem. Int. Ed.* **2016**, *55*, 3176–3180
Angew. Chem. **2016**, *128*, 3228–3232

[1] a) A. Fert, *Rev. Mod. Phys.* **2008**, *80*, 1517–1530; b) S. A. Wolf, D. D. Awschalom, R. A. Buhrman, J. M. Daughton, S. von Molnár, M. L. Roukes, A. Y. Chtchelkanova, D. M. Treger, *Science* **2001**, *294*, 1488–1495; c) X. Xu, W. Yao, D. Xiao, T. F. Heinz, *Nat. Phys.* **2014**, *10*, 343–350; d) M. R. Li, M. Retuerto, Z. Deng, P. W. Stephens, M. Croft, Q. Huang, H. Wu, X. Deng, G. Kotliar, J. Sanchez-Benitez, J. Hadermann, D. Walker, M. Greenblatt, *Angew. Chem. Int. Ed.* **2015**, *54*, 12069–12073; *Angew. Chem.* **2015**, *127*, 12237–12241.

[2] a) W. Han, R. K. Kawakami, M. Gmitra, J. Fabian, *Nat. Nanotechnol.* **2014**, *9*, 794–807; b) Y. Guo, J. Dai, J. Zhao, C. Wu, D. Li, L. Zhang, W. Ning, M. Tian, X. C. Zeng, Y. Xie, *Phys. Rev. Lett.* **2014**, *113*, 157202; c) M. Rein, N. Richter, K. Parvez, X.

Feng, H. Sachdev, M. Kläui, K. Müllen, *ACS Nano* **2015**, *9*, 1360 – 1366; d) X. Hong, S. H. Cheng, C. Herding, J. Zhu, *Phys. Rev. B* **2011**, *83*, 085410; e) R. R. Nair, M. Sepioni, I. L. Tsai, O. Lehtinen, J. Keinonen, A. V. Krasheninnikov, T. Thomson, A. K. Geim, I. V. Grigorieva, *Nat. Phys.* **2012**, *8*, 199 – 202.

[3] a) A. E. Berkowitz, J. R. Mitchell, M. J. Carey, A. P. Young, S. Zhang, F. E. Spada, F. T. Parker, A. Hutten, G. Thomas, *Phys. Rev. Lett.* **1992**, *68*, 3745 – 3748; b) B. J. Hickey, M. A. Howson, S. O. Musa, N. Wiser, *Phys. Rev. B* **1995**, *51*, 667 – 669; c) J. Q. Xiao, J. S. Jiang, C. L. Chien, *Phys. Rev. Lett.* **1992**, *68*, 3749 – 3752.

[4] G. Z. Magda, X. Jin, I. Hagymasi, P. Vancso, Z. Osvath, P. Nemes-Incze, C. Hwang, L. P. Biro, L. Tapaszto, *Nature* **2014**, *514*, 608 – 611.

[5] D. R. Dreyer, S. Park, C. W. Bielawski, R. S. Ruoff, *Chem. Soc. Rev.* **2010**, *39*, 228 – 240.

[6] a) Y. Liu, N. Tang, X. Wan, Q. Feng, M. Li, Q. Xu, F. Liu, Y. Du, *Sci. Rep.* **2013**, *3*, 2566; b) Y. Wang, Y. Huang, Y. Song, X. Zhang, Y. Ma, J. Liang, Y. Chen, *Nano Lett.* **2009**, *9*, 220 – 224.

[7] P. A. Denis, *J. Phys. Chem. C* **2009**, *113*, 5612 – 5619.

[8] P. Sun, K. Wang, J. Wei, M. Zhong, D. Wu, H. Zhu, *Nano Res.* **2014**, *7*, 1507 – 1518.

[9] K. N. Kudin, B. Ozbas, H. C. Schniepp, R. K. Prud'homme, I. A. Aksay, R. Car, *Nano Lett.* **2008**, *8*, 36 – 41.

[10] a) J. E. Hutchison, T. A. Postlethwaite, R. W. Murray, *Langmuir* **1993**, *9*, 3277 – 3283; b) J. Ji, G. Zhang, H. Chen, Y. Li, G. Zhang, F. Zhang, X. Fan, *J. Mater. Chem.* **2011**, *21*, 14498.

[11] U. Hartmann, *Annu. Rev. Mater. Sci.* **1999**, *29*, 53 – 87.

[12] a) H. Li, X. Qi, J. Wu, Z. Zeng, J. Wei, H. Zhang, *ACS Nano* **2013**, *7*, 2842 – 2849; b) V. F. Puntes, P. Gorostiza, D. M. Aruguete, N. G. Bastus, A. P. Alivisatos, *Nat. Mater.* **2004**, *3*, 263 – 268.

[13] a) G. Kresse, J. Furthmüller, *Comput. Mater. Sci.* **1996**, *6*, 15 – 50; b) G. Kresse, D. Joubert, *Phys. Rev. B* **1999**, *59*, 1758 – 1775.

[14] a) R. E. Camley, J. Barnaś, *Phys. Rev. Lett.* **1989**, *63*, 664 – 667; b) W. H. Butler, X. G. Zhang, D. M. C. Nicholson, J. M. MacLaren, *J. Magn. Magn. Mater.* **1995**, *151*, 354 – 362.

Received: December 9, 2015
Revised: January 15, 2016
Published online: January 28, 2016

